High Sensitivity Refractive Index Sensor Based on Trapezoidal Subwavelength Grating Slot Microring Resonator

Hanyue Li, Longsheng Wu, Yi Jin, and Aimin Wu

***Abstract*—High performance refractive index sensors are of important significance in numerous sensing applications including chemical, air and biophotonics. Among them, the ones with high sensitivity and large quality factor are especially critical. Here, we propose a high sensitivity refractive index sensor based on a slotted silicon ring resonator, of which the inner and outer rings are made of a deformed subwavelength grating (SWG) waveguide of trapezoidal dielectric blocks and a standard SWG waveguide of rectangular ones, respectively. By optimizing the geometry of inner silicon blocks, the quality factor is improved by 3 times than traditional subwavelength slot micro-ring resonator. The sensitivity of the single trapezoidal subwavelength grating slot microring resonator (T-SWGSMRR) sensor reaches 823 nm/RIU, with the Q factor of 2.5×10^4 and the limit of detection of 7.53×10^{-5} RIU are obtained. The sensitivity is further promoted by utilizing two cascaded T-SWGSMRRs on the basis of the Vernier effect, which reaches 12151 nm/RIU. The sensors presented in this work can be fabricated with commercial CMOS process, indicating that it has potential prospects in industrial applications.**

***Index Terms*—Refractive index sensor, silicon photonics, subwavelength grating, Vernier effect.**

I. Introduction

SILICON photonics integrated circuits (PICs), manufactured using the mature complementary metal-oxide-semiconductor (CMOS) technology, have gained the rapid development of low cost and monolithically integrated chips. These devices have sparked widespread research interest in investigating their various applications such as high-speed communication, sensing and signal processing. Refractive index (RI) sensors are widely recognized as an efficient technique for sensing gases, liquids, and biomolecules. Extensive research has been conducted on various fundamental components for the refractive index sensors, such as microring resonators (MRRs) [1], [2], [3], microdisks [4], [5] and photonic crystal devices [6], [7], [8]. In particular, MRRs has gained significant attention in refractive index sensing application due to their compact size and high Q resonance [9], [10]. High Q sensors offer the advantage of improving the limit of detection (LOD = λ/(Q•S), where S is the refractive index sensitivity), which enables the detection of extremely small changes in refractive index. However, these high Q sensors exhibit a small spectral shift when there are variations in the environmental refractive index, which is limited by the refractive index sensitivity. High refractive index sensitivity refers to the ability to convert a small change in the refractive index of the cladding analytes into a significant output signal, which is beneficial to amplify the sensing signal and improve signal processing. In addition, traditional silicon wire waveguides have a strong confinement of light due to the high refractive index contrast, which results in weak interaction between the electromagnetic field and the analyte. Consequently, sensors based on the traditional wire waveguides have the limited refractive index sensitivity.

Recently, the subwavelength grating (SWG) waveguide has been proposed and demonstrated for on-chip sensing [11]. The effective mode index of the SWG waveguide can be manipulated by designing the subwavelength unit cells. The sensitivity of the SWG-based refractive index sensor can also be enormously increased due to the less localization of electromagnetic field [12]. A SWG microring resonator (SWGMRR) was first demonstrated with the high sensitivity of 383 nm/RIU and the Q factor of 4×10^3 [13]. A trapezoidal SWGMRR(T-SWGMRR) improving the Q factor to 9.1×10^3 was proposed and the sensitivity was 440 nm/RIU [14]. A racetrack SWG slot MRR (R-SWGSMRR) was reported to enhance the sensitivity by using the SWGS waveguide, where the sensitivity is 1000 nm/RIU and Q factor is 5445 [15]. Nevertheless, the MRR sensor with high sensitivity usually has a lower mode field confinement, which results in the more bending loss and leads to a lower Q factor. For the present, the Q factor of the SWGSMRR sensors owning high sensitivity is limited by the more bending loss of the subwavelength grating slot (SWGS) waveguide.

In this work, the trapezoidal subwavelength grating slot micro-ring resonator (T-SWGSMRR) is proposed, which

Manuscript received 19 June 2023; accepted 21 June 2023. Date of publication 26 June 2023; date of current version 5 July 2023. This work was supported in part by the National Key R&D Program of China under Grant 2021YFB2206502, in part by Youth Innovation Promotion Association CAS under Grant 2021232, in part by the Program of Shanghai Academic Research Leader under Grant 22XD1404300, and in part by the National Natural Science Foundation of China under Grant 62275259. *(Corresponding authors: Yi Jin; Aimin Wu.)*

Hanyue Li, Longsheng Wu, and Aimin Wu are with the State Key Laboratory of Functional Materials for Informatics, Shanghai Institute of Microsystem and Information Technology, Chinese Academy of Sciences, Shanghai 200050, China, and also with the Center of Materials Science and Optoelectronics Engineering, University of Chinese Academy of Sciences, Beijing 100049, China (e-mail: hanyueli@mail.sim.ac.cn; wls502852331@mail.sim.ac.cn; wuaimin@mail.sim.ac.cn).

Yi Jin is with the Centre for Optical and Electromagnetic Research and International Research Center for Advanced Photonics, College of Optical Science and Engineering, Zhejiang University, Hangzhou 310058, China (e-mail: jinyi_2008@zju.edu.cn).

Digital Object Identifier 10.1109/JPHOT.2023.3289336

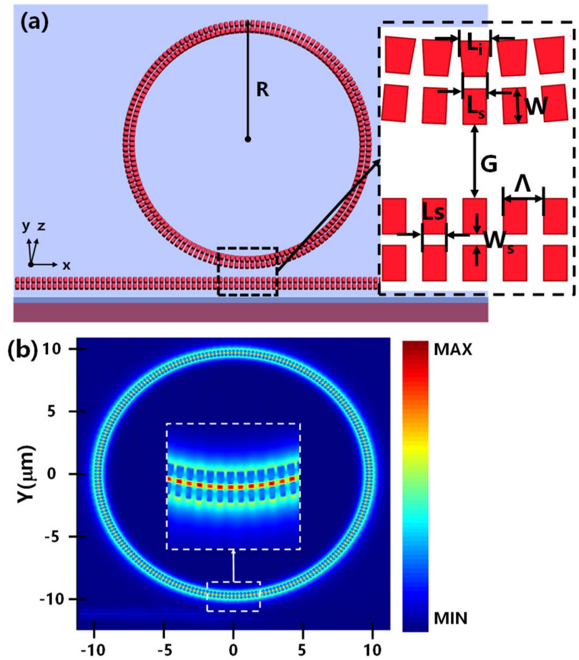

Fig. 1. (a) 3D schematic of the proposed T-SWGSMRR sensor and the grating period (Λ), the rectangle length (L_s), the inner trapezoidal length (L_i), the block width (W), the slot width (W_s) and the gap (G) between the bus waveguide and the ring waveguide are shown in the inset. (b) Electric profile of the T-SWGSMRR at the resonant wavelength.

utilizing trapezoidal silicon blocks in the inner ring SWG waveguide to acquire the large Q factor and the high sensitivity. The silicon blocks of the inner ring SWG waveguide are designed to be trapezoidal to diminish the bending loss of light field and enhance the interaction between light and analytes using the SWGS waveguide. The influences of the structural parameters on the sensitivity and the quality factor are investigated. The high refractive index sensitivity of 823 nm/RIU and a large quality factor of 2.50×10^4 are achieved in the single T-SWGSMRR sensor with optimized design. Furthermore, the two cascaded T-SWGSMRRs sensor based on the Vernier effect is designed to further enhance the sensitivity to 12151 nm/RIU, which is higher than previous studies and paves the way for sensing applications with ultra-low refractive index changes.

II. Design Principles and Optimizations

The three-dimensional (3D) schematic of the T-SWGSMRR sensor is shown in Fig. 1(a). The device is designed on a SOI substrate, which consists of a top silicon layer of 220 nm and a buried oxide layer of 2 μm. The geometric parameters of the T-SWGSMRR are denoted in the inset, including the grating period (Λ), the rectangle length (L_s), the inner trapezoidal length (L_i), the block width (W), the slot width (W_s) and the gap (G) between the bus and the ring waveguide. The radius (R) of the T-SWGSMRR is chosen as 10 μm for low bending loss. To ensure the SWGS waveguide works in the subwavelength regime ($\lambda/\Lambda >> 2n_{eff}$, $\lambda = 1550$ nm) and considering the restriction of minimum feature size, the grating period Λ is set to 280 nm.

TABLE I
Correspondence Between Refractive Index and Concentration of the Sodium Chloride Solutions At Room Temperature

Concentration	0%	1%	2%	3%	4%
Refractive index	1.333	1.3348	1.3366	1.3384	1.3402

In SWGSMRR sensors constructed with rectangular blocks, the mode field in the slot tends to be skewed towards the outer ring due to the bending effect of the ring SWGS waveguide, leading to increased losses and a decreased Q factor. To address this issue, an asymmetric ring SWGS structure with a longer inner trapezoidal length ($L_i > L_s$) is employed to confine the light wave along the center of the slot, and the electric field distribution of the T-SWGSMRR at the resonant wavelength is in Fig. 1(b). By implementing this design, the Q factor of the T-SWGSMRR is improved.

Refractive index sensitivity and Q factor are two key parameters that characterize optical refractive index sensors. Refractive index sensitivity is defined as the ratio of the change of the resonance wavelength (Δλ) around 1550 nm to the corresponding refractive index change (Δn_c) of the cladding material outside the device ($S_c = \Delta\lambda/\Delta n_c$). The transmission spectrum properties and the limit of detection ($LOD = \lambda/(Q \bullet S_c)$) are largely determined by the Q factor ($Q = \lambda/FWHM$, where FWHM is the full width at half maximum of the transmission spectrum of MRRs). In the design of the T-SWGSMRR, four structural parameters play a decisive role in the performances, which are the duty cycle ($dc = L_s/\Lambda$) of the SWGS waveguide, the block width (W), the slot width (W_s) of the SWGS waveguides, and the inner trapezoidal length (L_i).

In the analysis of the refractive index sensing performance of the device, sodium chloride (NaCl) solutions with different concentrations are employed as the cladding analytes. The corresponding relation between the concentration of NaCl solution and refractive index is presented in Table I. The refractive index of the solution could be varied from 1.333 to 1.3402 by adjusting the concentration from 0% to 4%. Here the 2.5D finite time domain difference algorithm in MODE solver is used for simulation to balance the computational memory requirements and the accuracy of the results. The mesh size is set to $\Delta x = \Delta y = 10$ nm, $\Delta z = 20$ nm, the simulation time is 200000 fs and the minimum spectral step is 5 pm. These simulation conditions ensure a reliable and efficient simulation process for analyzing the T-SWGSMRR's refractive index sensing capabilities.

Fig. 2(a) shows the dependence of refractive index sensitivity of the T-SWGSMRR sensor on the duty cycles (dc) of the SWGS wavelength at a fixed W = 220 nm, $W_s = 80$ nm and $L_i = 200$ nm. As the duty cycle is reduced from 0.7 to 0.4, the light field distributed in the low refractive index materials becomes stronger, resulting in an increased overlap between the analyte and the light, thus leading to a stronger light-matter interaction and a higher sensitivity of the sensor. However, the lower duty cycle can also result in increased propagation loss in the SWGS waveguide, which leads to a decrease in the Q factor and a higher LOD. For instance, when the duty cycle (dc) of the

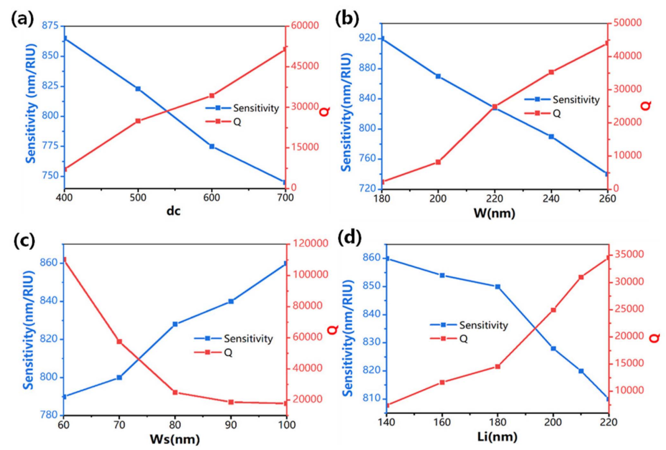

Fig. 2. (a) Sensitivity of the T-SWGSMRR sensor with different duty cycle (dc). Sensitivity and Q factor of the T-SWGSMRR under (b) different block width (W), (c) different slot width (W_s) and (d) different inner trapezoidal length (L_i).

SWG waveguide is increased from 0.4 to 0.5, the Q factor rises significantly from 7045 to 24941 at the resonant wavelength closest to 1550 nm, while the sensitivity only decreases slightly from 865 nm/RIU to 823 nm/RIU. However, further increasing the duty cycle to 0.6 and 0.7, the sensitivity observably decreases to 780 nm and 740 nm, respectively. Therefore, the duty cycle of the SWG waveguide is set to 0.5 to achieve a balance between sensitivity and Q factor, i.e., $L_s = 140$ nm.

The variations of refractive index sensitivity and Q factor with the block width (W) at $L_s = 140$ nm, $W_s = 80$ nm and $L_i = 200$ nm are depicted in Fig. 2(b). Decreasing the block width from 220 nm to 200 nm leads to an increase in sensitivity and a decrease in Q factor due to less localized light and increased bending loss of the T-SWGSMRR, in which the Q factor decrease quickly and is lower than 20000. In addition, increasing the block width from 220 nm to 260 nm results in reducing sensitivity from 823 nm/RIU to 740 nm/RIU and rising Q factor due to more localized light and less bending loss. Considering the influence of W on the sensitivity and Q factor, W is chosen as 220 nm to obtain a high sensitivity and a large Q factor.

Fig. 2(c) shows the influence of the slot width (W_s) on refractive index sensitivity and Q factor with $L_s = 140$ nm, $W = 220$ nm and $L_i = 200$ nm. The sensitivity increases linearly with an increase of W_s because light field distribution in the analyte becomes stronger, while the Q factor decreases as the W_s increases. Furthermore, the fabrication of the device becomes challenging as the W_s decreases. The structural tolerance of Q factor at $W_s = 70$ nm is worse than that at $W_s = 80$ nm, in addition, the Q factor at $W_s = 90$ nm is less than 20000. Therefore, a balance needs to be made between sensitivity enhancement, Q factor degradation and fabrication difficulty. The results demonstrate that the T-SWGSMRR refractive index sensor can achieve high sensitivity while maintaining an acceptable Q factor by setting the slot width to 80 nm.

The performances dependence with the inner trapezoidal length (L_i) are illustrated in Fig. 2(d). The fixed parameters are

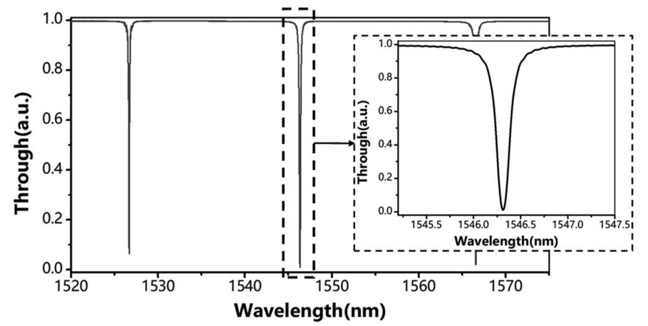

Fig. 3. Transmission spectrum of the T-SWGSMRR sensor with $L_s = 140$ nm, $W_s = 80$ nm, $W = 220$ nm and $L_i = 200$ nm.

$L_s = 140$ nm, $W = 220$ nm and $W_s = 80$ nm. The variation trends of the sensitivity and Q factor to L_i are opposite, that is due to the effective mode index raising with the L_i increase. A decrease in the effective mode index leads to an enhanced delocalization of the mode field, causing an increase in the sensitivity, and a decrease in the Q factor due to increased bending loss from the weaker confinement of the mode field. The Q value of the SWGSMRR based on the inner trapezoidal blocks with $L_i = 200$ nm is 3 times larger than that of the MRR based on the inner rectangular blocks with $L_i = 140$ nm. In addition, the inner trapezoidal length has a nonnegligible impact on the gap between two inner blocks. The gap between inner blocks is 70 nm when L_i is 200 nm, and the minimum feature size becomes narrower with L_i continuing to increase. Considering the difficulty of device fabrication and the trade-off between sensitivity enhancement and Q factor degradation with L_i increasing, L_i is set to 200 nm.

From these above optimizations, these structural parameters of the T-SWGSMRR sensor are determined: $L_s = 140$ nm, $W_s = 80$ nm, $W = 220$ nm and $L_i = 200$ nm. To acquire the sensor with these optimized parameters in the manufacturing process, multiple groups device structures with varying sizes around optimized parameters need be fabricated to compensate for potential fabrication errors of sizes. Moreover, refer to the device fabrication method used in reference [17], devices with a minimum feature size of 60 nm are guaranteed precisely. Therefore, the T-SWGSMRR sensor with optimized parameters can be achieved precisely.

III. Results and Discussions

Fig. 3 illustrates the simulated transmission spectrum of the T-SWGSMRR exposed to deionized water with an 800 nm gap between the bus waveguide and the ring waveguide. Notably, the T-SWGSMRR achieves the resonant wavelength (λ) of 1546.31 nm, the extinction ratio (ER) of 20.2 dB and the full width of half maximum (FWHM) of 0.062 nm. Furthermore, the T-SWGSMRR exhibits a calculated Q factor of 24941.

Fig. 4(a) depicts the simulated transmission spectrums of the T-SWGSMRR device when exposed to NaCl solutions of different concentrations at room temperature. The initial transmission spectrum is shown with a central wavelength of 1546.31 nm at a cladding refractive index of 1.333. By increasing the refractive indexes of the solution to 1.3348, 1.3366, 1.3384 and 1.3402,

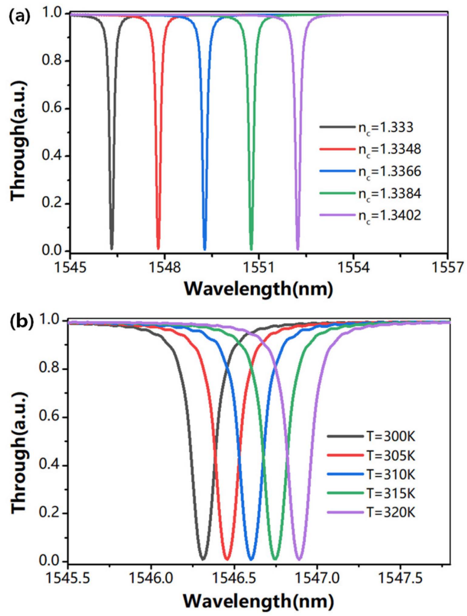

Fig. 4. Transmission spectrums of the T-SWGSMRR sensor with (a) the different cladding refractive indexes and (b) the different temperatures.

the device spectra shift to 1547.79 nm, 1549.27 nm, 1550.75 nm and 1552.25 nm, respectively. This clearly indicates that even a small change in the refractive index of the analytes induces a noticeable shift in the wavelength of the resonant peak. The device exhibited a refractive sensitivity of 823 nm/RIU and a LOD of 7.53×10^{-5} RIU based on calculations.

The through transmission spectrums of the T-SWGSMRR sensor when exposed to deionized water at different temperatures are shown in Fig. 4(b). As the chip temperature rises from 300 K to 320 K with a step of 5 K, the device spectra exhibit a corresponding shift from 1546.31 nm to 1546.89 nm. The temperature sensitivity of the device is determined to be 29 pm/K, which makes it suitable for temperature compensation in the device test system.

The refractive index sensitivity of the T-SWGSMRR sensor is 823 nm/RIU, which is higher than that of wire MRRs and SWGMRR [10], [13]. The Q factor of the T-SWGSMRR on the use of inner trapezoidal blocks is improved 3 times more than that of the SWGSMRR utilizing conventional rectangular blocks. However, although the sensitivity of the T-SWGSMRR can reach 823 nm/RIU, it is constrained by the structure due to the substantial propagation loss of the SWGS waveguide caused by excessively small dielectric blocks. During the test process, the microfluidic-channel technology can be used in the sensing experiment to force the solution to penetrate into the gaps. The pressure of the solution is exerted on the chip, which results from the fast-flow rate of the solution through the small-size microfluidic channel. This technology has reached a high level of maturity in the sensing testing based on SWGs, and its implementation has produced experimental results consistent with the simulated prediction [16], [17], [18]. In addition, the temperature controller is employed to rigorously control the chip temperature throughout the testing phase.

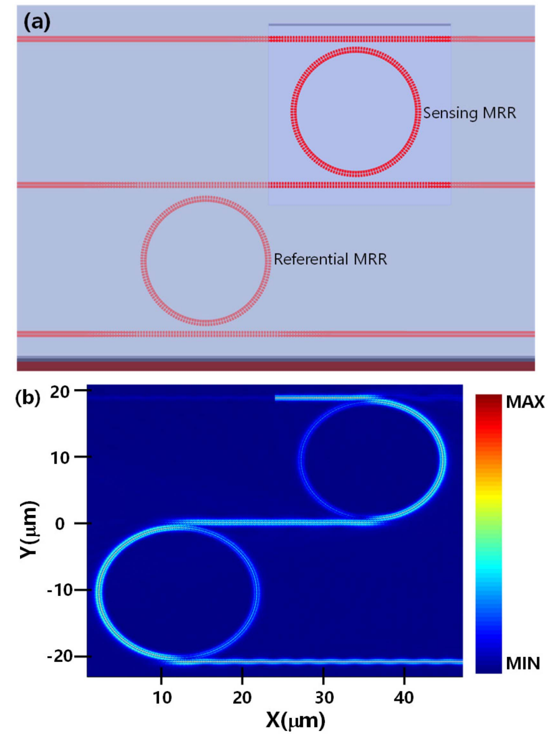

Fig. 5. (a) Structural diagram and (b) normalized electric field distribution diagram of the two cascaded T-SWGSMRRs sensor.

IV. Principle and Results of Two Cascaded Micro-Rings Sensor

To overcome the limitation of refractive index sensitivity in the T-SWGSMRR structure, a novel cascaded-type refractive index sensor is designed on the basis of the Vernier effect. This sensor is formed by cascading two T-SWGSMRRs, which includes a sensing MRR and a referential MRR, as shown in Fig. 5(a). The Vernier effect is a phenomenon in sensing applications that describes the effective improvement of sensors' sensitivity realized by utilizing two transmission spectrums with slightly different FSRs [19].

To achieve the Vernier effect, the free spectral ranges (FSR_s and FSR_r) of the two rings are intentionally designed to have a slight difference. This is accomplished by selecting different radius (R_s and R_r) for the sensing ring and the referential ring. Given the optimized structural parameters of the above single T-SWGSMRR sensor, certain structural parameters of the two cascaded MRRs remain unchanged and are as follows: the block width of 200 nm, the grating period of 280 nm, the duty cycle of 0.5 and the slot width of 80 nm. The radius and the gap between the bus waveguide and the ring waveguide of the sensing ring are 10 μm and 700 nm, respectively. The radius and the gap between the bus waveguide and the ring waveguide of the referential ring are 9 μm and 400 nm, respectively. The transmission of the cascaded light field is shown in Fig. 5(b), in which the light is input at the upper-left port of the sensing MRR and output at the lower-right drop port of the referential MRR.

When the two cascaded T-SWGSMRRs sensor is immersed in NaCl solutions with different concentrations, the sensing MRR

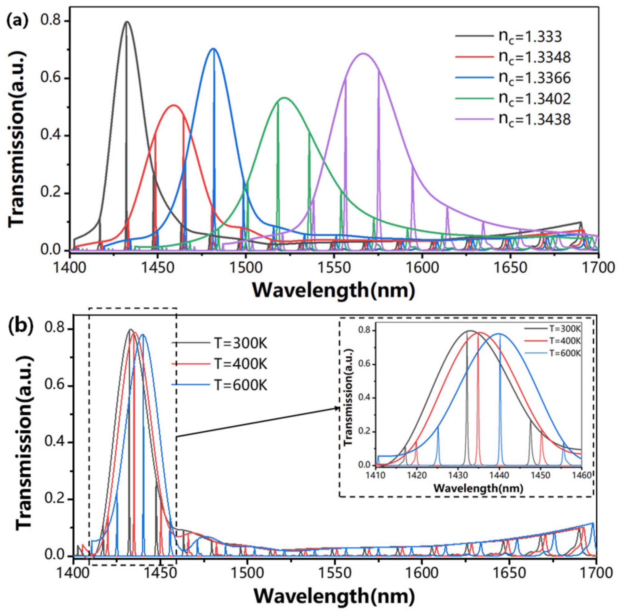

Fig. 6. Transmission spectrums of the two cascaded T-SWGSMRRs sensors varied with (a) the different refractive indexes and (b) the different temperatures.

TABLE II
PERFORMANCE COMPARISON OF RECENT MICRORING-BASED REFRACTIVE INDEX SENSORS WITH DIFFERENT TYPES OF WAVEGUIDES

Device structure	Sensitivity (nm/RIU)	Q	LOD (RIU)	Radius (μm)	Cladding	Reference
R-SWGSMRR	429.7	9.8×10^3	3.71×10^{-4}	10	Water	[20]*
SWGMRR	383	4×10^3	N/A	10	Water	[13]*
A-SWGSMRR	672.8	33864	6.69×10^{-5}	10	Air	[21]
SWGSMRR	490	7×10^3	5.5×10^{-4}	30	Water	[22]*
Fano-SWGMRR	366	N/A	N/A	5	Water	[23]*
T-SWGMRR	440	9.1×10^3	3.9×10^{-4}	10	Water	[14]*
Double slot-R-SWGSMRR	1000	5445	3.12×10^{-4}	5	Air	[15]
Slot MRR	476	1.9×10^3	1.7×10^{-3}	30	Water	[24]*
SWGMRR	600	N/A	N/A	10	Air	[25]
R-SWGMMR	664	15918	1.43×10^{-4}	10	Water	[26]
Single T-SWGSMRR	823	2.50×10^4	7.53×10^{-5}	10	Water	This work
Cascaded MRRs	3456	2×10^4	1.15×10^{-2}	264	Water	[27]*
Cascaded MRRs	5866	N/A	N/A	138	Water	[28]*
MRR-MZI	3552	N/A	N/A	40	Water	[29]*
Cascaded R-SWGSMMR	7061	12500	1.74×10^{-5}	10	Water	[26]
Cascaded T-SWGSMRRs	12151	4.78×10^3	2.47×10^{-5}	10	Water	This work

[a] The reference with * is the experimental results.

(without the SiO_2 cladding) interacts strongly with the NaCl solutions, whereas the referential MRR (covered by a SiO_2 cladding) maintains a stable transmission spectrum. The transmission spectrum of the cascaded sensor is the multiplicative result of the transmission spectra of the two cascaded MRRs, which results in a multiplied sensitivity. The wavelength shift ($\Delta\lambda_t$) of the two cascaded T-SWGSMRRs sensor is

$$\Delta\lambda_t = \Delta\lambda_s \cdot \frac{FSR_r}{|FSR_r - FSR_s|}$$

Where $\Delta\lambda_s$ is the wavelength shift of the sensing MRR cascaded by the refractive index change of the cladding analyte. The refractive index sensitivity (S_{tc}) of the cascade sensor is defined as the ratio of the shift ($\Delta\lambda_s$) of the resonant wavelength at the cascade sensor's drop port to the change (Δn_c) of the refractive index of the analyte,

$$S_{tc} = \frac{\Delta\lambda_s}{\Delta n_c} = S_{sc} \cdot \frac{FSR_r}{|FSR_r - FSR_s|}$$

Where S_{sc} is the refractive index sensitivity of the single sensing T-SWGSMRR. The refractive index sensitivity of the two cascaded T-SWGSMRRs sensor is magnified by a gain factor of $G = FSR_r / |FSR_r - FSR_s|$ as compared to that of the single sensing micro-ring resonator. The FSR of the two cascaded micro-rings sensor is given by $FSR_t = G \cdot FSR_s$.

The FSR of the referential MRR is 21.2 nm according to our simulation, while that of the sensing MRR is 20.24 nm from the above analysis of a single T-SWGSMRR. By calculating and employing the gain factor of G = 22.08, the FSR of the two cascaded T-SWGSMRRs sensor is calculated to be 446.9 nm. The output transmission spectra of the two cascaded micro-rings sensors in NaCl solutions with different concentrations at room temperature are shown in Fig. 6(a). In deionized water, the initial peak wavelength of the envelope spectrum is 1433 nm with a Q factor of 4777. As the refractive indexes of the NaCl solutions change to 1.3348, 1.3366, 1.3402, and 1.3438, the corresponding shifted peak wavelengths of the envelope spectrums are observed to be 1458 nm, 1481 nm, 1522 nm, and 1566 nm, respectively. The refractive index sensitivity of the cascaded sensor is calculated to be 12151 nm/RIU, which indicates distinct advantages for high-resolution environmental monitoring and biosensing. When the chip temperatures heat up to 400 K and 600 K, the corresponding shifted peak wavelengths are 1435.2 nm and 1439.5 nm, respectively, as shown in Fig. 6(b). Consequently, the temperature sensitivity of the cascaded sensor is calculated to be 21.6 nm/K.

The performances of recent MRR-based refractive index sensors are listed in Table II. Our single T-SWGSMRR sensor shows a Q factor of 2.5×10^4, sensitivity of 823 nm/RIU, and LOD of 7.53×10^{-5} RIU. The refractive index of the single T-SWGSMRR is higher than wire MRRs and SWGMRRs that have been reported and the Q factor is larger than most present SWG-based MRRs in references [13], [14], [20], [21], [22], [23], [24], [25], [26]. Our designed devices require a processing technology of 70 nm, which decreases the fabrication difficulties and ensure feasibility through the use of a well-established manufacturing process. There have been many experimental articles focusing on SWG microring sensers [13], [14], [20], [23], and the fabrication technology of SWG has achieved a relatively mature state. Furthermore, the performance of the two cascaded T-SWGSMRRs sensor is also evaluated, which exhibits a high sensitivity of 12151 nm/RIU. This sensitivity is 1.7∼3.5 times larger than the previous cascaded two MRRs sensor [26], [27], [28], [29].

V. CONCLUSION

In summary, we have proposed a high-performance refractive index sensor based on a T-SWGSMRR. By introducing trapezoidal silicon blocks into the inner SWG waveguide allows for smooth modulation of the effective mode index along the radial direction to reduce the bend leakage. Theoretically, the designed T-SWGSMRR possesses a large Q factor of 2.50×10^4, a high sensitivity of 823 nm/RIU, and a low LOD of 7.53×10^{-5} RIU. Further, by utilizing the Vernier effect, the sensor based on two cascaded T-SWGSMRRs is demonstrated to further improve the sensitivity to 12151 nm/RIU and lower the LOD to 2.47×10^{-5} RIU. The current work presents a significant improvement on sensitivity and enables a promising candidate for practical applications such as water monitoring and disease diagnosis.

References

[1] S. M. C. Abdulla et al., "Sensing platform based on micro-ring resonator and on-chip reference sensors in SOI," *Proc. SPIE*, vol. 8990, pp. 190–195, 2014.

[2] L. Guan, Z. Wang, G. Yuan, Y. Chen, L. Dong, and Z. Peng, "Sensing performance of micro-ring differential optical biosensor," *Infrared Laser Eng.*, vol. 47, no. 2, pp. 0222002–1–0222002–6, 2018.

[3] P. Steglich et al., "Silicon photonic micro-ring resonators for chemical and biological sensing: A tutorial," *IEEE Sensors J.*, vol. 22, no. 11, pp. 10089–10105, Jun. 2022.

[4] V. M. N. Passaro, B. Casamassima, F. De Leonardis, F. Dell'Olio, and F. Magno, "Modeling and design of a microdisk photonic sensor for biological applications," in *Proc. IEEE 2nd Int. Workshop Adv. Sensors Interface*, 2007, pp. 1–6.

[5] S. Yegnanarayanan, W. Roman, M. Soltani, G. Cremona, H. Lu, and A. Adibi, "On-chip integration of microfluidic channels with ultra-high Q silicon microdisk resonators for lab-on-a-chip sensing applications," in *Proc. IEEE Lasers Electro-Opt. Soc. Annu. Meeting Conf.*, 2007, pp. 50–51.

[6] J. García-Rupérez et al., "Label-free antibody detection using band edge fringes in SOI planar photonic crystal waveguides in the slow-light regime," *Opt. Exp.*, vol. 18, no. 23, pp. 24276–24286, 2010.

[7] B. Troia, A. Paolicelli, F. De Leonardis, and V. M. Passaro, "Photonic crystals for optical sensing: A review," in *Advances in Photonic Crystals*. Boca Raton, FL, USA: CRC Press, 2013, pp. 241–295.

[8] A. K. Goyal and S. Pal, "Design and simulation of high sensitive photonic crystal waveguide sensor," *Optik*, vol. 126, no. 2, pp. 240–243, 2015.

[9] W. Bogaerts et al., "Silicon microring resonators," *Laser Photon. Rev.*, vol. 6, no. 1, pp. 47–73, 2012.

[10] J. Niehusmann, A. Vörckel, P. H. Bolivar, T. Wahlbrink, W. Henschel, and H. Kurz, "Ultrahigh-quality-factor silicon-on-insulator microring resonator," *Opt. Lett.*, vol. 29, no. 24, pp. 2861–2863, 2004.

[11] J. G. Wangueemert-Perez et al., "Evanescent field waveguide sensing with subwavelength grating structures in silicon-on-insulator," *Opt. Lett.*, vol. 39, no. 15, pp. 4442–4445, Aug. 2014.

[12] Z. S. Ruan, L. Shen, S. Zheng, and J. Wang, "Subwavelength grating slot (SWGS) waveguide on silicon platform," *Opt. Exp.*, vol. 25, no. 15, pp. 18250–18264, Jul. 2017.

[13] V. Donzella, A. Sherwali, J. Flueckiger, S. M. Grist, S. T. Fard, and L. Chrostowski, "Design and fabrication of SOI micro-ring resonators based on sub-wavelength grating waveguides," *Opt. Exp.*, vol. 23, no. 4, pp. 4791–4803, Feb. 2015.

[14] H. Yan et al., "Unique surface sensing property and enhanced sensitivity in microring resonator biosensors based on subwavelength grating waveguides," *Opt. Exp.*, vol. 24, no. 26, pp. 29725–29734, Dec. 2016.

[15] N. L. Kazanskiy, S. N. Khonina, and M. A. Butt, "Subwavelength grating double slot waveguide racetrack ring resonator for refractive index sensing application," *Sensors*, vol. 20, no. 12, Jun. 2020, Art. no. 3416.

[16] L. Huang, H. Yan, L. Xiang, N. Zhou, D. He, and X. Mi, "Subwavelength racetrack resonators with enhanced critically coupled tolerance for on-chip sensing," *IEEE Access*, vol. 9, pp. 23424–23431, 2021.

[17] E. X. Luan, H. Yun, M. L. Ma, D. M. Ratner, K. C. Cheung, and L. Chrostowski, "Label-free biosensing with a multi-box sub-wavelength phase-shifted Bragg grating waveguide," *Biomed. Opt. Exp.*, vol. 10, no. 9, pp. 4825–4838, Sep. 2019.

[18] E. Luan et al., "Enhanced sensitivity of subwavelength multibox waveguide microring resonator label-free biosensors," *IEEE J. Sel. Topics Quantum Electron.*, vol. 25, no. 3, May/Jun. 2019, Art. no. 7300211.

[19] O. Schwelb and I. Frigyes, "Vernier operation of series-coupled optical microring resonator filters," *Microw. Opt. Technol. Lett.*, vol. 39, no. 4, pp. 257–261, Nov. 2003.

[20] L. J. Huang et al., "Improving the detection limit for on-chip photonic sensors based on subwavelength grating racetrack resonators," *Opt. Exp.*, vol. 25, no. 9, pp. 10527–10535, May 2017.

[21] N. Wu and L. Xia, "Side-mode suppressed filter based on anangular grating-subwavelength grating microring resonator with high flexibility in wavelength design," *Appl. Opt.*, vol. 58, no. 26, pp. 7174–7180, Sep. 2019.

[22] J. Flueckiger et al., "Sub-wavelength grating for enhanced ring resonator biosensor," *Opt. Exp.*, vol. 24, no. 14, pp. 15672–15686, Jul. 2016.

[23] Z. R. Tu, D. S. Gao, M. L. Zhang, and D. M. Zhang, "High-sensitivity complex refractive index sensing based on Fano resonance in the subwavelength grating waveguide micro-ring resonator," *Opt. Exp.*, vol. 25, no. 17, pp. 20911–20922, Aug. 2017.

[24] V. Mere, H. Muthuganesan, Y. Kar, C. V. Kruijsdijk, and S. K. Selvaraja, "On-chip chemical sensing using slot-waveguide-based ring resonator," *IEEE Sensors J.*, vol. 20, no. 11, pp. 5970–5975, Jun. 2020.

[25] Y. M. Xu, C. Y. Fu, S. B. Sun, and M. Kong, "Wide-range refractive index sensing relied on tracking the envelope spectrum of a dispersive subwavelength grating microring resonator," *Opt. Laser Technol.*, vol. 154, Oct. 2022, Art. no. 108304.

[26] L. Liu, Z. Hu, M. Ye, Z. Yu, C. Ma, and J. Li, "On-chip refractive index sensor with ultra-high sensitivity based on sub-wavelength grating racetrack microring resonators and Vernier effect," *IEEE Photon. J.*, vol. 14, no. 5, Oct. 2022, Art. no. 6849007.

[27] L. Jin, M. Y. Li, and J. J. He, "Highly-sensitive silicon-on-insulator sensor based on two cascaded micro-ring resonators with Vernier effect," *Opt. Commun.*, vol. 284, no. 1, pp. 156–159, Jan. 2011.

[28] Y. Liu, Y. Li, M. Y. Li, and J. J. He, "High-sensitivity and wide-range optical sensor based on three cascaded ring resonators," *Opt. Exp.*, vol. 25, no. 2, pp. 972–978, Jan. 2017.

[29] Y. Zhang, J. Zou, Z. Cao, and J. J. He, "Temperature-insensitive waveguide sensor using a ring cascaded with a Mach-Zehnder interferometer," *Opt. Lett.*, vol. 44, no. 2, pp. 299–302, Jan. 2019.